nature genetics

SUPPLEMENTARY INFORMATION

https://doi.org/10.1038/s41588-019-0360-8

In the format provided by the authors and unedited.

Chromosome segregation errors generate a diverse spectrum of simple and complex genomic rearrangements

Peter Ly[1,9]*, Simon F. Brunner[2], Ofer Shoshani[1], Dong Hyun Kim[1], Weijie Lan[1], Tatyana Pyntikova[3], Adrienne M. Flanagan[4,5], Sam Behjati[2,6], David C. Page[3,7,8], Peter J. Campbell[2] and Don W. Cleveland[1]*

[1]Ludwig Institute for Cancer Research, Department of Cellular and Molecular Medicine, University of California San Diego School of Medicine, La Jolla, CA, USA. [2]Wellcome Sanger Institute, Hinxton, UK. [3]Whitehead Institute for Biomedical Research, Cambridge, MA, USA. [4]University College London Cancer Institute, London, UK. [5]Department of Histopathology, Royal National Orthopaedic Hospital NHS Trust, Stanmore, UK. [6]Department of Paediatrics, University of Cambridge, Cambridge, UK. [7]Howard Hughes Medical Institute, Whitehead Institute for Biomedical Research, Cambridge, MA, USA. [8]Department of Biology, Massachusetts Institute of Technology, Cambridge, MA, USA. [9]Present address: Department of Pathology, University of Texas Southwestern Medical Center, Dallas, TX, USA. *e-mail: peter.ly@utsouthwestern.edu; dcleveland@ucsd.edu

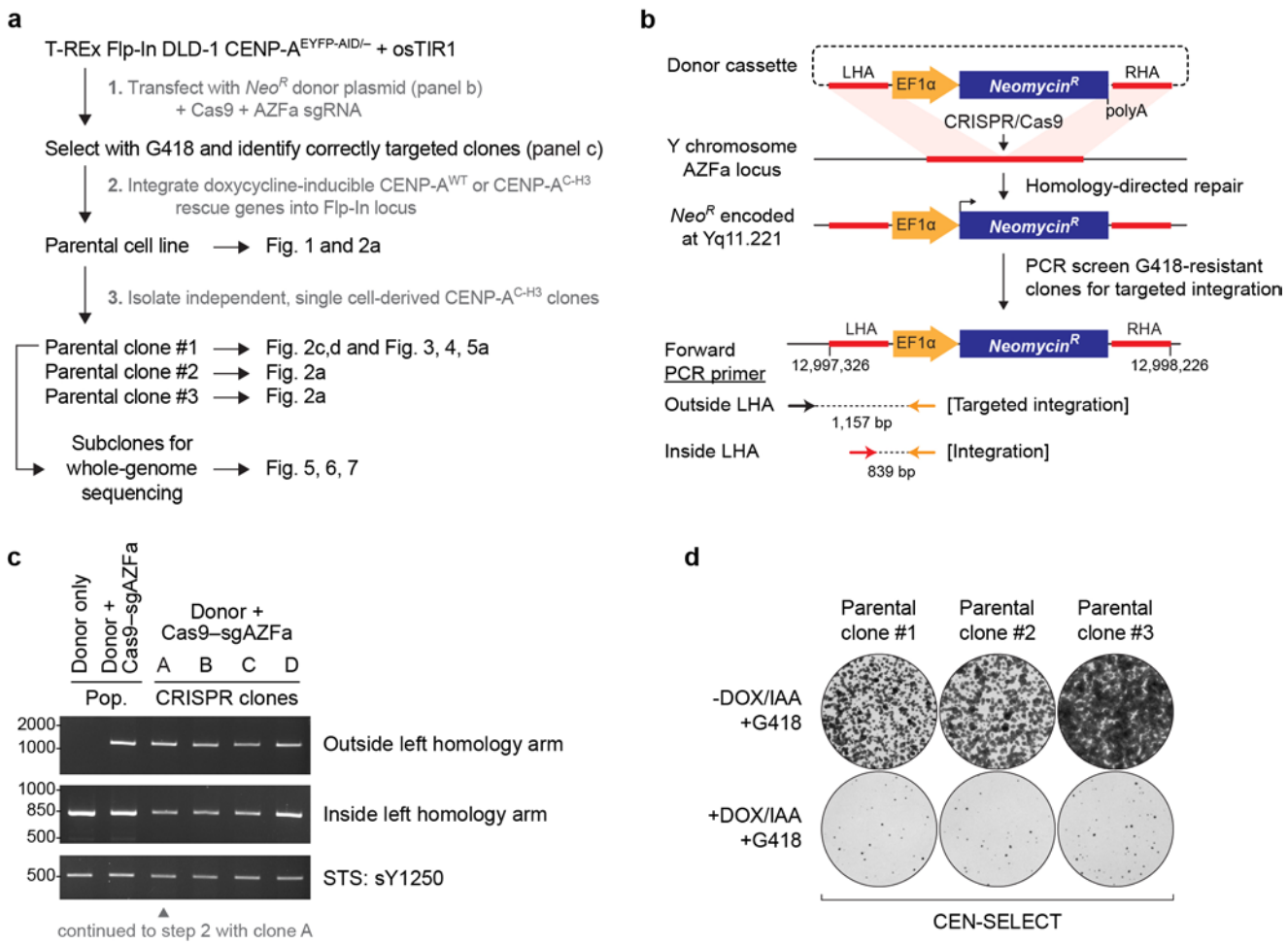

Supplementary Figure 1

CRISPR–Cas9-mediated engineering of a neomycin-resistance gene (*Neo*^{R}) into the Y chromosome AZFa locus.

a) Step-by-step outline of genome editing strategies used to generate DLD-1 cells and their corresponding clonal derivatives used in this study. *Neo*^{R}, neomycin-resistance gene. **b)** Schematic of CRISPR/Cas9-mediated integration of *Neo*^{R} into the Y-chromosome AZFa locus. The locations of PCR primers used to identify clones with correct *Neo*^{R} integration are shown. Forward primers outside the left homology arm (HA) produced a PCR product specific for correct integration. As a control, another set of forward primers within the left HA amplified both correct and non-specific integration events. Coordinates represent reference assembly GRCh38. **c)** PCR using the primers shown in **b** or the indicated sequence-tagged site (STS). Four correctly targeted clones were identified, of which the indicated clone was chosen for further modifications, as shown in **a**. **d)** Representative colony formation plate scans (n = 3 biological replicates) from 3 independent DLD-1 clones carrying a CENP-A$^{C–H3}$ rescue gene, which were generated as described in **a,** following the indicated treatment conditions.

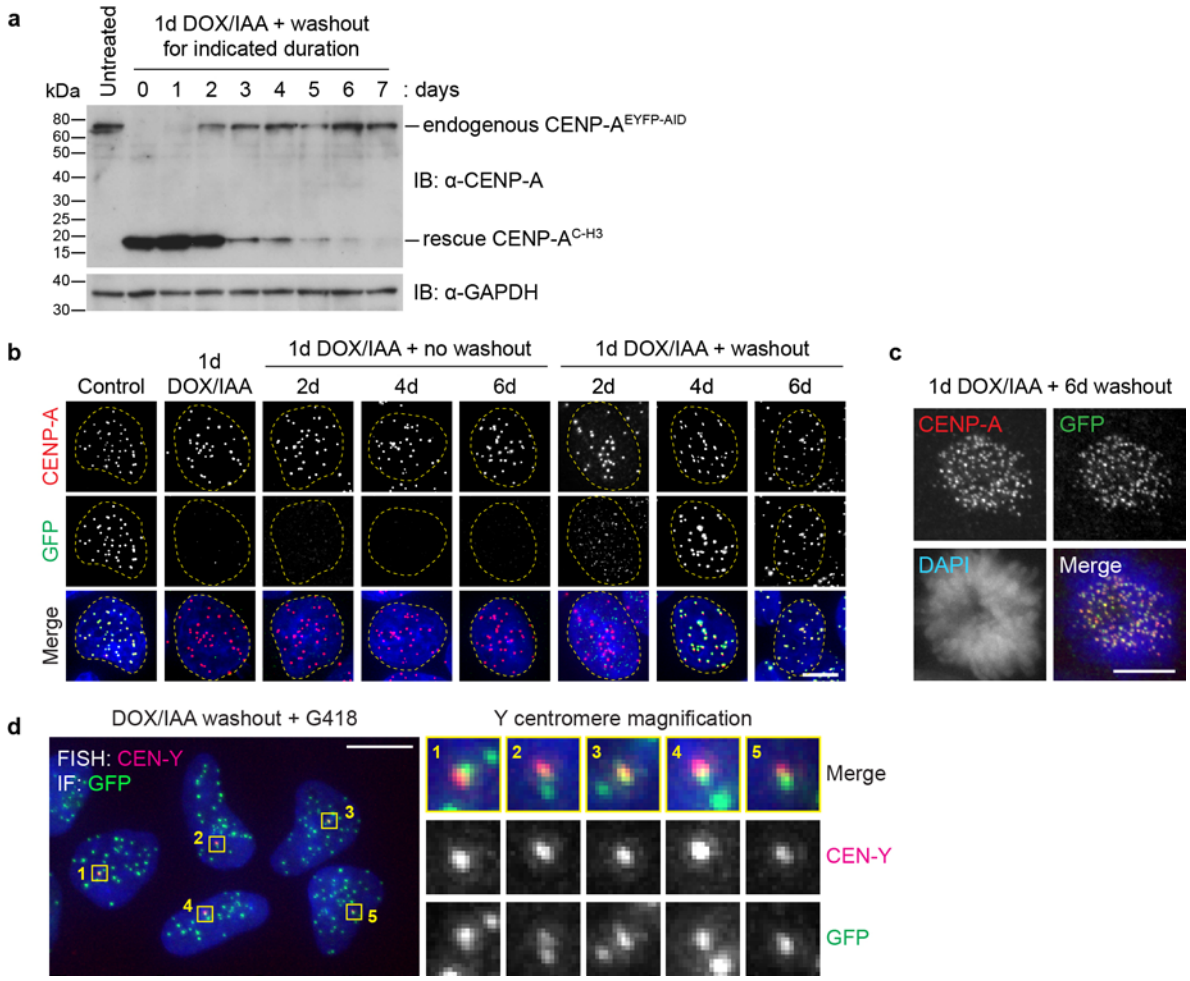

Supplementary Figure 2

Endogenous CENP-A reaccumulates and localizes to the Y chromosome centromere after doxycycline/auxin washout.

a-c) DLD-1 cells carrying a CENP-A$^{C–H3}$ rescue gene were treated with or without DOX/IAA followed by washout for the indicated duration. **a)** Whole-cell lysates were immunoblotted with antibodies against CENP-A or GAPDH as a loading control. **b,c)** Representative immunofluorescence images using antibodies against CENP-A and GFP on **b)** interphase cells or **c)** mitotic cells. Anti-GFP antibody specifically recognizes endogenous, wild-type CENP-A fused to an EYFP-AID tag. Scale bars, 5 µm. **d)** DLD-1 cells carrying a CENP-A$^{C–H3}$ rescue gene were treated with DOX/IAA for 3d followed by 4d washout and selection in G418 for 10d. Cells were processed for immunofluorescence with a GFP antibody, followed by DNA FISH using a Y centromere-specific probe. Magnified insets show positive GFP signals detected at the Y centromere. Scale bar, 10 µm.

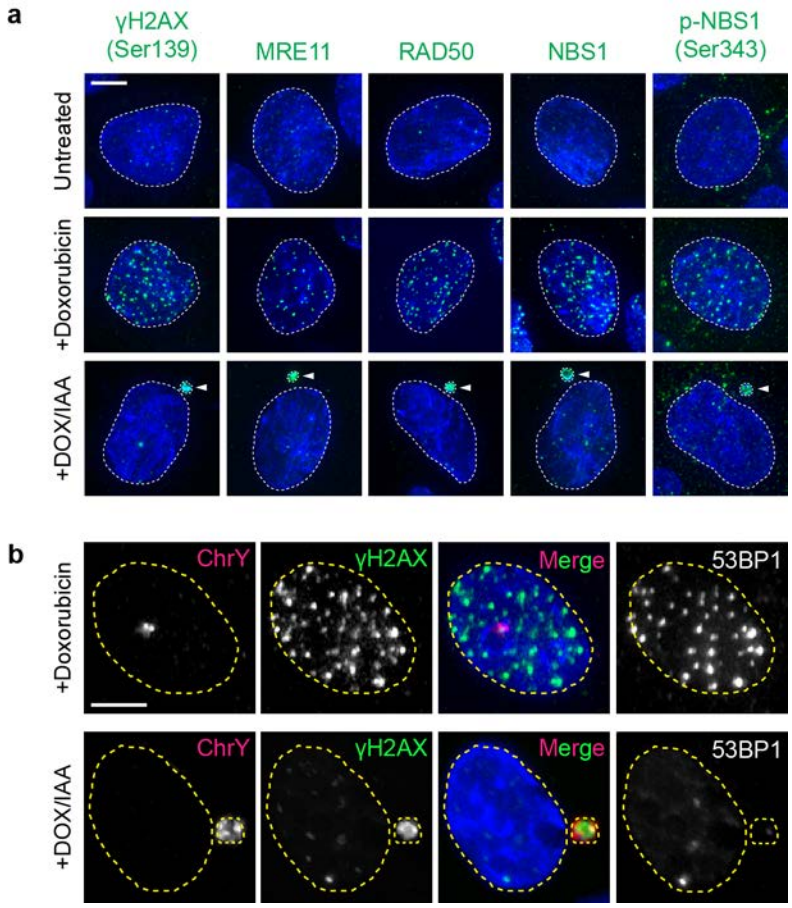

Supplementary Figure 3

Recognition of micronuclear DNA damage without active DNA double-strand-break repair.

a) Representative immunofluorescence images of DLD-1 cells treated with 1 µM doxorubicin for 1h or DOX/IAA for 3d stained with antibodies against the indicated DNA damage components. Scale bar, 5 µm. **b)** Representative immuno-FISH images of DLD-1 cells treated with 1 µM doxorubicin for 1h or DOX/IAA for 3d. Cells were processed for immunofluorescence with γH2AX and 53BP1 antibodies followed by DNA FISH using a Y chromosome paint probe. Scale bar, 5 µm.

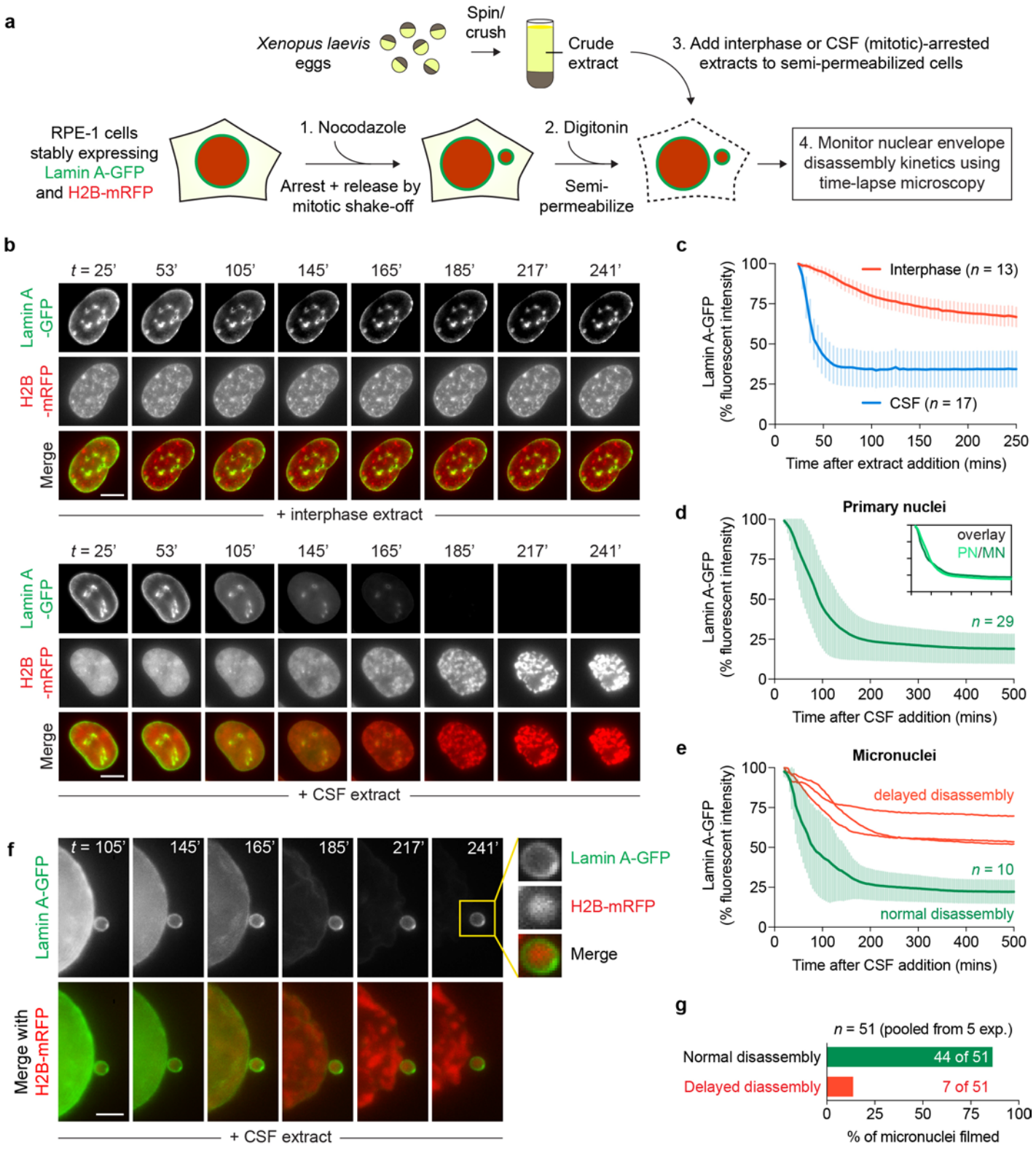

Supplementary Figure 4

Most micronuclei disassemble their nuclear envelopes with normal kinetics during mitotic entry.

a) Experimental schematic for nuclear envelope breakdown assay using *Xenopus* egg extracts, which contain abundant kinases whose activity can disassemble typical nuclear membranes and promote chromosome condensation, the latter visualized by H2B–mRFP. **b)** Time-lapse imaging of semi-permeabilized RPE-1 cells expressing lamin A–GFP and H2B–mRFP following the addition of interphase or CSF-arrested egg extracts. Scale bar, 5 µm. **c)** Lamin A–GFP disassembly kinetics following the addition of interphase or CSF-arrested egg extract (mean ± SEM). **d-e)** Lamin A–GFP disassembly kinetics following CSF-arrested egg extract addition for **d)** primary nuclei and **e)** micronuclei. Inset depicts the overlay between primary nuclei and micronuclei with normal disassembly. Green lines represent mean ± SEM, and red lines indicate individual examples of micronuclei with partial or delayed lamin A–GFP disassembly. **f)** Example image series of a micronucleus that fails to efficiently disassemble its nuclear envelope upon addition of CSF-arrested egg extracts. Scale bar, 2 µm. **g)** Quantification of the frequency of micronuclei undergoing normal or delayed disassembly in the presence of CSF-arrested egg extracts. Data in **c-e** and **g** represent *n* = number of nuclei or micronuclei as indicated.

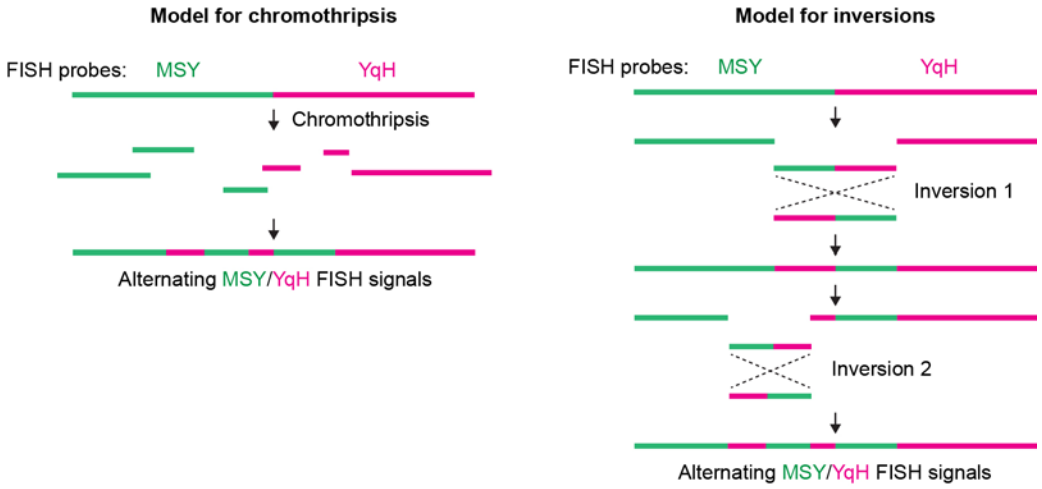

Supplementary Figure 5

Schematic for the generation of alternating FISH patterns by chromothripsis or a series of inversions.

(associated with Figure 2d)

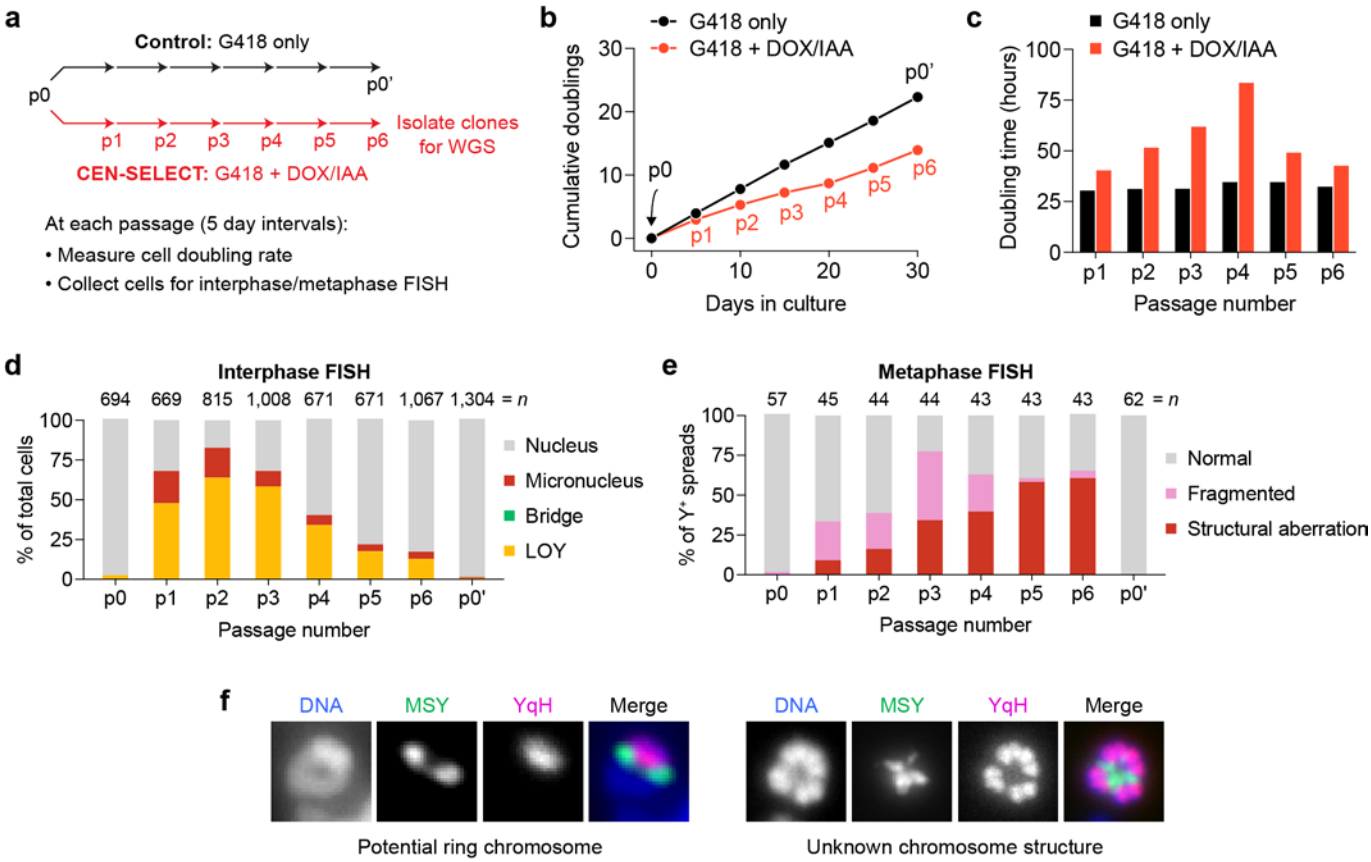

Supplementary Figure 6

Population dynamics during chronic centromere inactivation and selection.

a) Experimental schematic for chronic centromere inactivation. p, passage; p0, starting population; p0', final passage of cells selected with G418 without Y centromere inactivation. **b-c)** Measurements of **b)** cumulative cell doublings and **c)** population doubling time at each passage. **d)** Quantification of Y chromosome location from interphase cells hybridized to whole Y chromosome paint probes (*n* = number of cells examined). **e)** Quantification of Y chromosome structural status from metaphase spreads hybridized to MSY/YqH FISH probes (*n* = number of metaphases examined). **f)** Examples of a rare ring chromosome and uncharacterized derivative chromosome following prolonged CEN-SELECT.

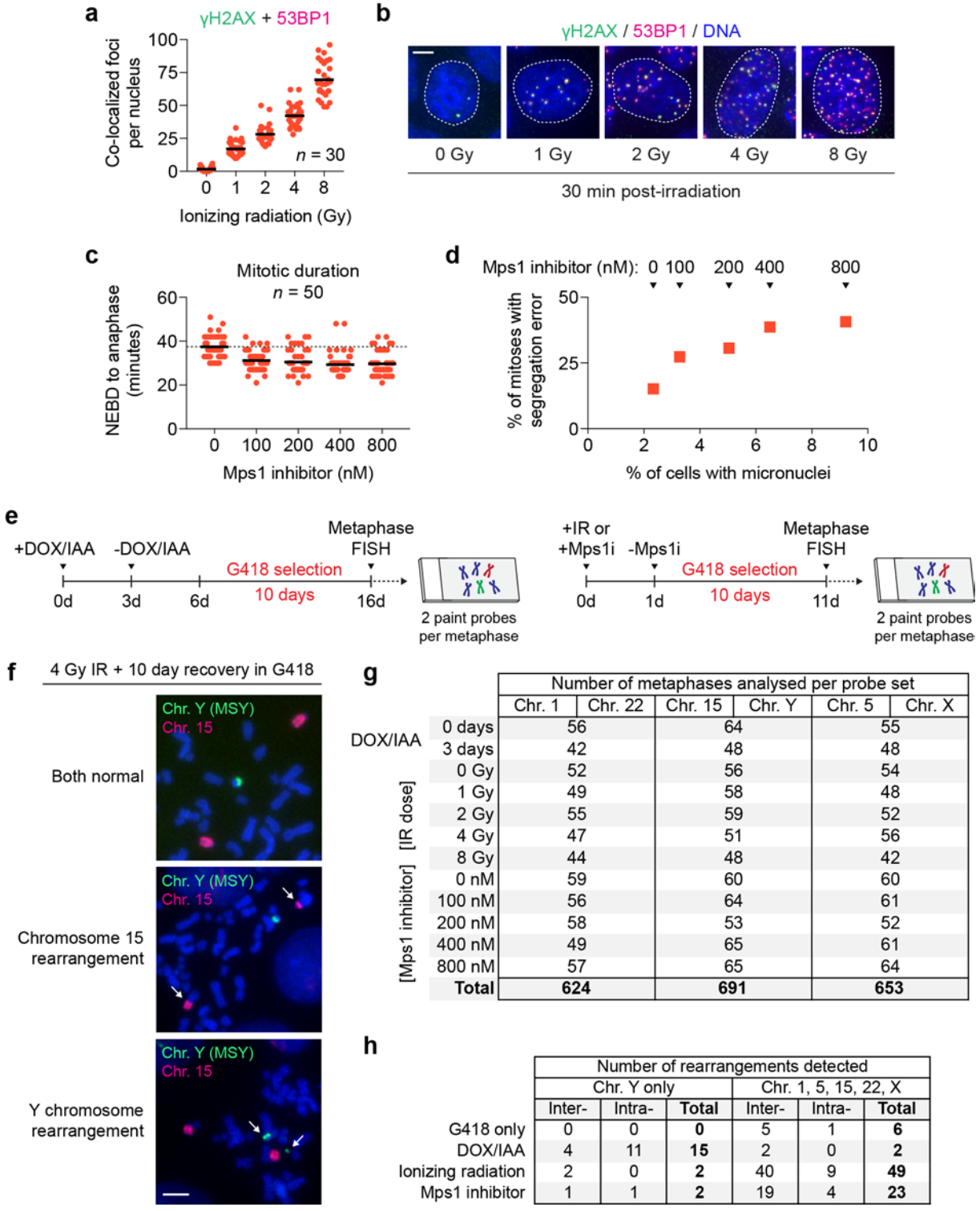

g

		Number of metaphases analysed per probe set					
		Chr. 1	Chr. 22	Chr. 15	Chr. Y	Chr. 5	Chr. X
DOX/IAA	0 days	56		64		55	
	3 days	42		48		48	
[IR dose]	0 Gy	52		56		54	
	1 Gy	49		58		48	
	2 Gy	55		59		52	
	4 Gy	47		51		56	
	8 Gy	44		48		42	
[Mps1 inhibitor]	0 nM	59		60		60	
	100 nM	56		64		61	
	200 nM	58		53		52	
	400 nM	49		65		61	
	800 nM	57		65		64	
Total		**624**		**691**		**653**	

h

	Number of rearrangements detected					
	Chr. Y only			Chr. 1, 5, 15, 22, X		
	Inter-	Intra-	**Total**	Inter-	Intra-	**Total**
G418 only	0	0	**0**	5	1	**6**
DOX/IAA	4	11	**15**	2	0	**2**
Ionizing radiation	2	0	**2**	40	9	**49**
Mps1 inhibitor	1	1	**2**	19	4	**23**

Supplementary Figure 7

Chromosomal rearrangements generated from ionizing-radiation exposure or mitotic spindle assembly checkpoint inactivation.

(associated with Figure 4a)

a-b) Increasing doses of ionizing radiation were used to induce widespread DNA damage, which produced co-localized nuclear foci of γH2AX and 53BP1. DLD-1 cells were treated with the indicated doses of radiation and fixed after recovery for 30 minutes. Cells were processed for immunofluorescence using antibodies against γH2AX and 53BP1. Quantification of co-localized foci (*n* = number of cells examined per dose) is shown in **a**, and representative images are shown in **b**. Scale bar, 5 μm. **c-d)** An inhibitor of the Mps1 mitotic kinase (reversine) was used to inactivate the spindle assembly checkpoint during mitosis to drive premature anaphase onset. DLD-1 cells stained with SiR-DNA were treated with the indicated doses of reversine and imaged by time-lapse microscopy. Quantification of mitotic duration is shown in **c** (*n* = number of cells examined per dose; NEBD, nuclear envelope breakdown), and the frequency of mitotic events developing chromosome segregation errors is shown in **d**. At the highest concentration used (800 nM), nearly half of mitoses resulted in errors with micronuclei detected in ~10% of cells. **e)** Experimental schematic for Figure 4a. **f)** Examples of irradiated cells showing structural rearrangements for the indicated chromosomes by metaphase FISH. Scale bar, 5 μm. **g)** Sample sizes for each condition and set of probes for Figure 4a. **h)** The total number of inter- and intra-chromosomal rearrangements observed for the indicated conditions.

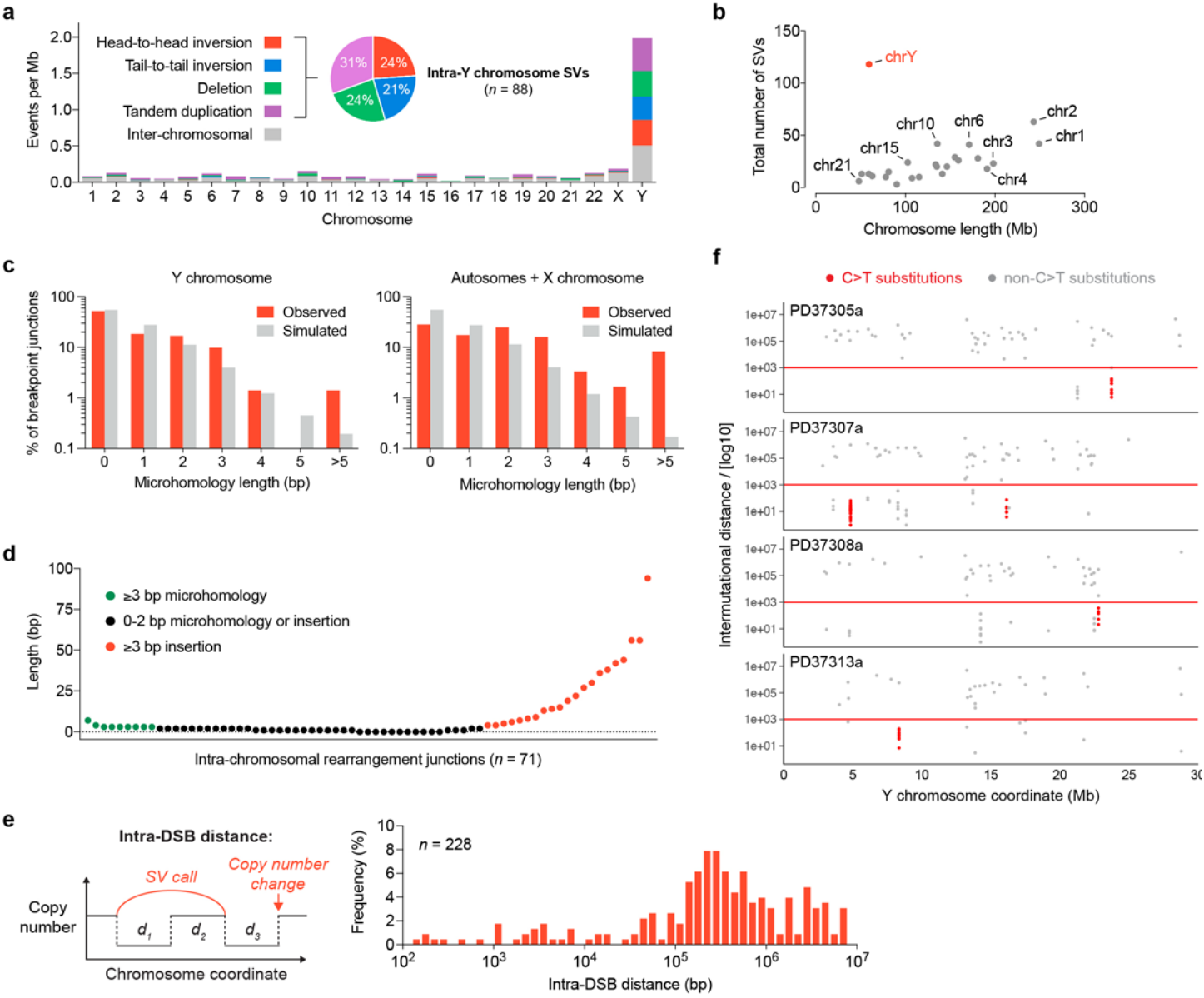

Supplementary Figure 8

Molecular sequence features of chromosomal-rearrangement breakpoint junctions.

a) Bar graph depicting the total number of structural variants detected per chromosome normalized to chromosome size and copy-number. Data were pooled from all 20 sequenced clones. Inner pie chart shows the distribution of each Y-Y junction orientation. **b)** Scatter plot depicting the absolute number of structural variants per chromosome compared to its length. **c)** Distribution of 71 breakpoints reconstructed from 817 split-end reads with the indicated lengths of microhomology for Y-chromosome specific or non-Y chromosome junctions compared to microhomology lengths from 7,100 randomly simulated junctions (see **Online Methods**). Data were compiled from all sequenced clones. **d)** Distribution of microhomology or insertion lengths with each dot representing an individually reconstructed Y-Y breakpoint junction. **e)** Schematic of intra-DSB distance measurements (left) and distribution of Y chromosome fragment sizes pooled across all sequenced clones (right). **f)** Rainfall plot of substitution patterns across the MSY region from four clones. Red dots below the line represent sites of consecutive C>T basepair substitutions with a 1 kb intermutation distance.

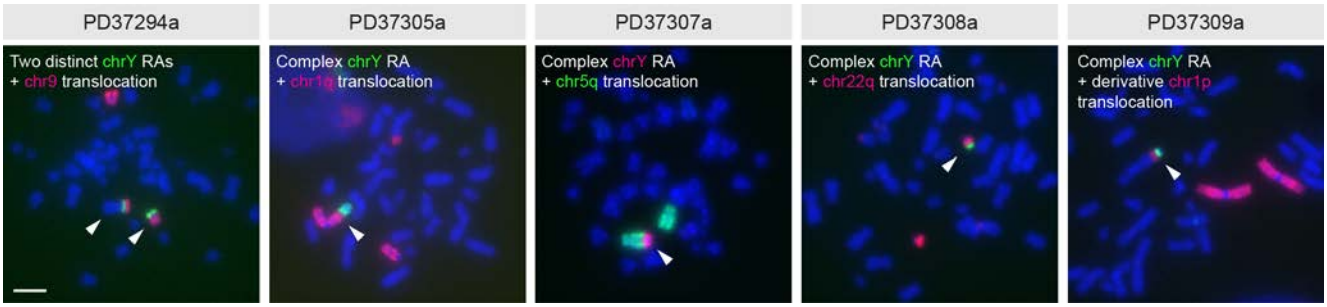

Supplementary Figure 9

Cytogenetic verification of rearrangement partners identified by whole-genome sequencing.

Representative metaphase FISH images of the indicated clones hybridized to the corresponding chromosome paint probes. Scale bar, 5 µm.

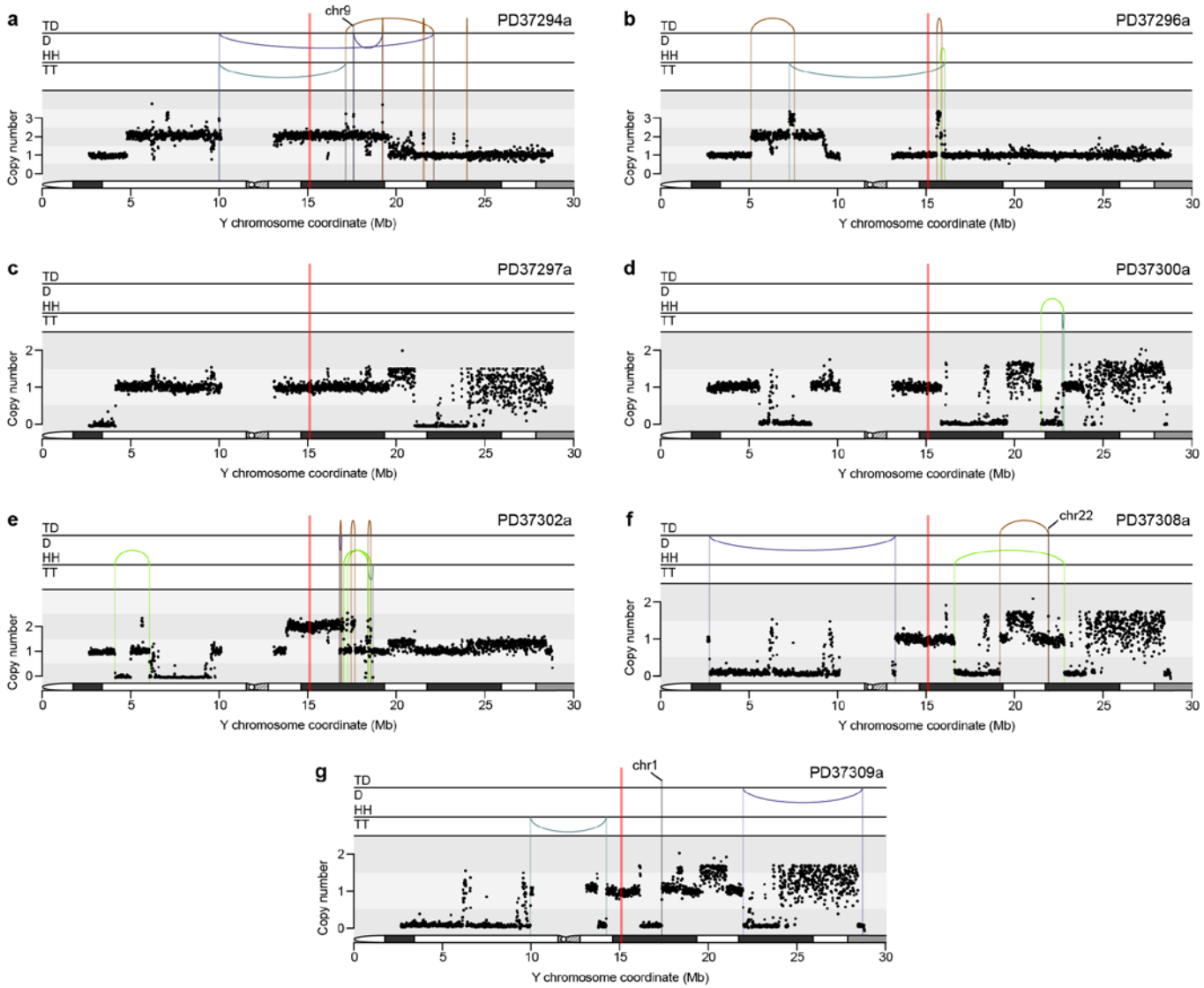

Supplementary Figure 10

Y chromosome rearrangement and DNA copy-number profiles of additional clones.

Red vertical line indicates position of the integrated *Neo*^{R} gene. All three inter-chromosomal translocations shown were confirmed by metaphase FISH. X-axes are clipped at 30 Mb to exclude the Yq heterochromatic region.

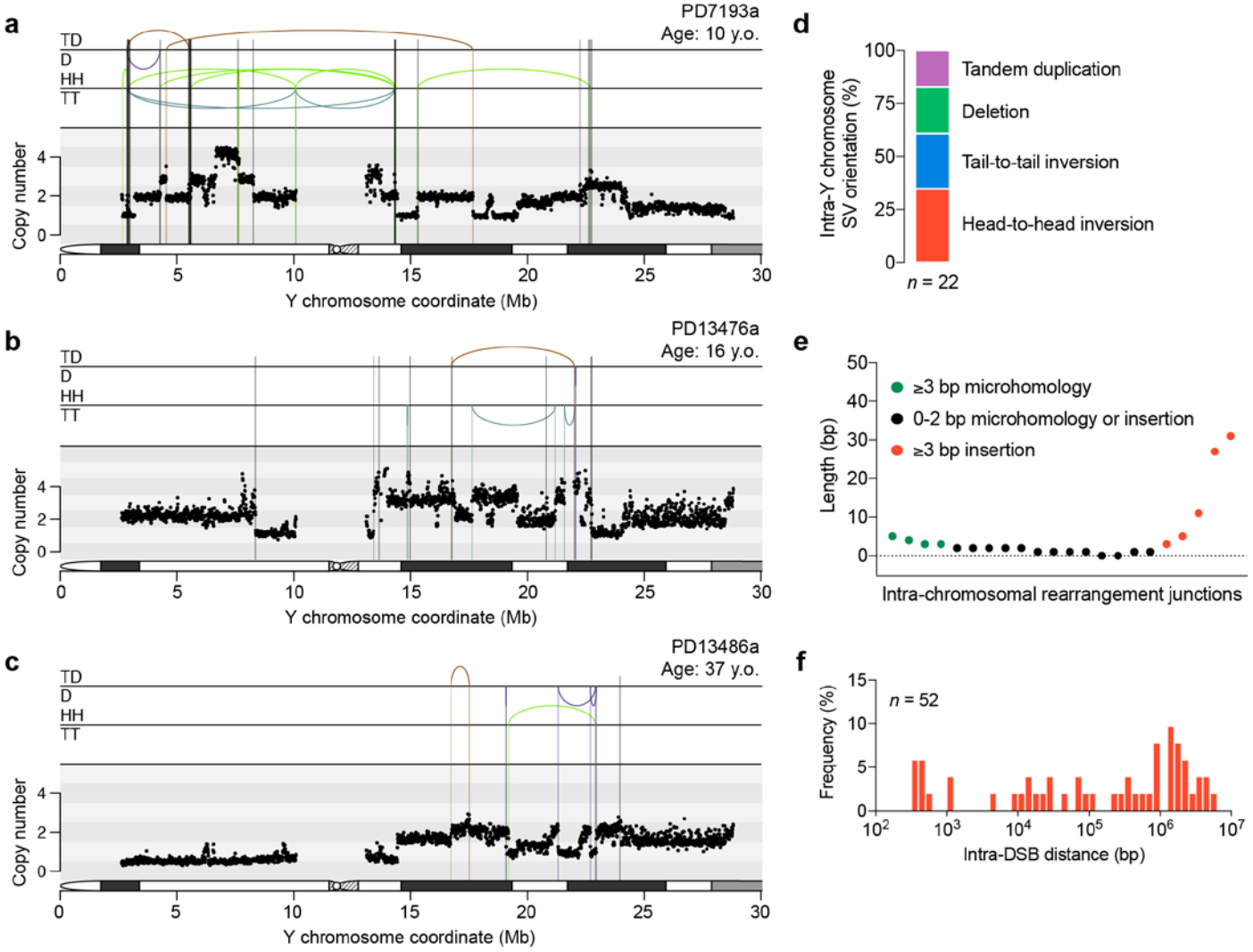

Supplementary Figure 11

Patients with osteosarcoma presenting complex Y chromosome rearrangements coupled to interchromosomal translocations.

a-c) X-axes are clipped at 30 Mb to exclude the Yq heterochromatic region. Vertical grey lines represent inter-chromosomal rearrangements with **a)** chromosome 11, **b)** chromosomes 1, 19, and 22, and **c)** chromosome 15. **d)** Distribution of each Y-Y junction orientation (*n* = number of breakpoint junctions). **e)** Distribution of microhomology or insertion lengths with each dot representing an individually reconstructed Y-Y breakpoint junction. **f)** Distribution of intra-DSB distances pooled across all three examples.

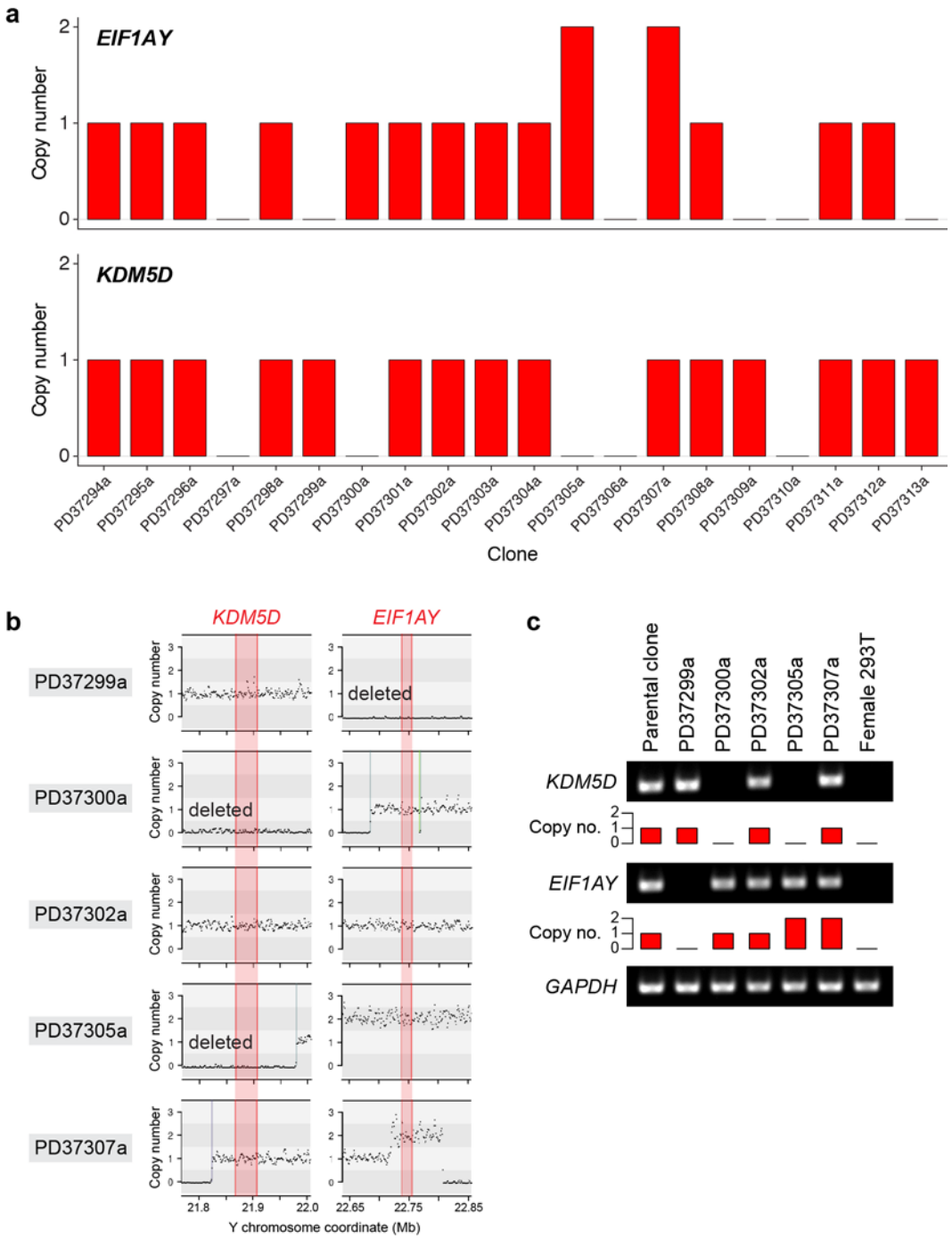

Supplementary Figure 12

DNA copy-number analyses of two somatically expressed Y chromosome genes.

a) DNA copy-number plots for *KDM5D* and *EIF1AY* across all clones obtained by sequencing. **b)** Magnified DNA copy-number profiles at the *KDM5D* or *EIF1AY* gene regions, represented by red shading, in the indicated clones. **c)** Reverse transcription polymerase chain reaction (RT-PCR) analysis of *KDM5D*, *EIF1AY*, or *GAPDH* transcripts from the indicated clones or female HEK-293 cells as a negative control. Bar graphs show the copy-number status of the respective gene.

SUPPLEMENTARY INFORMATION LIST

Supplementary Figures 1-12

Supplementary Note

Supplementary Videos 1-2

Supplementary Tables 1-3

SUPPLEMENTARY NOTE

Description of rearrangement types identified using MSY/YqH FISH probes

Inter-chromosomal rearrangements comprised three categories: (1) *End-fusions* occurred when a complete copy of the Y chromosome joined a non-homologous chromosome in its entirety at or near the telomeres without the net loss of DNA sequence, which can produce a pseudodicentric chromosome. (2) *Translocations* occurred when a portion of the Y joined another chromosome at a distal region with deletion of the Y sequences that did not participate in the translocation event, the majority of which were non-reciprocal in nature. Because the MSY probe cannot distinguish the Yp arm from the proximal Yq arm, we considered a translocation to occur at Yp when the FISH signal nearest the translocation breakpoint hybridized to the euchromatic MSY portion of the Y chromosome, and conversely, to Yq when hybridized to the YqH probe. In contrast to translocations, (3) *insertions* occurred when a fragment of the Y joined an interstitial portion of another chromosome.

Intra-chromosomal rearrangements comprised four additional categories: (4) *Complex* patterns of rearrangements were observed in which the MSY/YqH FISH signals overlapped extensively, appeared highly diffused, and/or created ambiguous configurations wherein the breakpoints and rearrangement patterns were not easily discernible by microscopy. We predict a fraction of these to be chromothriptic in nature, which would require next-generation DNA sequencing to resolve. (5) Some derivative chromosomes were characterized by patterns that seemingly alternated between MSY/YqH signals, producing a banded appearance along the chromosomal axis. These rearrangements can either be explained by chromothripsis, or alternatively, by a series of *inversions* spanning the euchromatic MSY and YqH regions (see **Supplementary Fig. 5**). (6) *Isodicentrics* appeared as two copies of the Y fused to form a mirror-imaged duplication at either the Yp or Yq arm, a potential byproduct of sister chromatid recombination. Among all isodicentrics observed, none were joined at opposite Y arms (i.e., fusion between Yp/Yq ends). Lastly, (7) *deletions* occurred when one or both arms appeared truncated. The resolution of microscopy-based FISH permitted the detection of large, distal deletions, with small and/or internal deletions not readily visible.

SUPPLEMENTARY DATA

Supplementary Video 1 | Normal micronuclear envelope disassembly during mitosis. Time-lapse imaging of DLD-1 lamin A–GFP cell entering mitosis with a micronucleus, indicated by a white arrow (6 minutes/frame, mean intensity projection). Note that the major nucleus and micronucleus undergoes concurrent nuclear envelope breakdown upon mitotic entry.

Supplementary Video 2 | Aberrant micronuclear envelope disassembly during mitosis. Time-lapse imaging of DLD-1 lamin A–GFP cell entering mitosis with a micronucleus, indicated by a white arrow (6 minutes/frame, mean intensity projection). Note that the micronucleus fails to undergo proper nuclear envelope breakdown throughout mitosis and persists into the subsequent cell cycle.

Supplementary Table 1 | Summary of DLD-1 clones analysed by cytogenetics and whole-genome sequencing.

Supplementary Table 2 | Breakpoint junctions with microhomology or non-templated DNA insertion sequences.

Supplementary Table 3 | List of primer sequences.